ScenarioCLIP: Pretrained Transferable Visual Language Models and Action-Genome Dataset for Natural Scene Analysis

Advik Sinha Saurabh Atreya Aashutosh A V Sk Aziz Ali Abhijit Das Machine Intelligence Group, Department of CS&IS, Birla Institute of Technology and Science, Pilani – Hyderabad Campus

abhijit.das@hyderabad.bits-pilani.ac.in

Abstract

Until recently, the general corpus of CLIP-type fundamental models has widely explored either the retrieval of short descriptions or the classification of objects in the scene as SINGLE-object image classification task. The same holds for retrieving the image embedding (image retrieval task) given a text prompt. However, real-world scene images exhibit rich compositional structure involving multiple objects and actions. The latest methods in the CLIP-based literature improve class-level discrimination by mining harder negative image-text pairs and by refining permanent text prompts, often using LLMs. However, these improvements remain confined to predefined class lists and do not explicitly model relational or compositional structure. Pyramid-CLIP partially addresses this gap by aligning global and local visual features, yet it still lacks explicit modeling of inter-object relations. Hence, to further leverage this aspect for scene analysis, the proposed model ScenarioCLIP accepts input texts, grounded relations, and input images, along with focused regions highlighting relations to separate disentangled encoders. Feature alignment is performed with the contrastive cross-alignment, and an Exponential Moving Average (EMA)-based knowledge distillation is performed between the global level, and finer object and relation levels within each modality. The proposed ScenarioCLIP model is pretrained on curated scenario data, and finetuned for specialized downstream tasks, such as cross-modal retrieval and fine-grained visual understanding tasks. Along with the ScenarioCLIP model, to address the lack of domain-specific datasets, we generate a novel dataset by extending image-text pairs from existing diverse indoor and outdoor scenario datasets that are publicly available, such as OpenPSG, Panoptic Video Scene Graph, Kinetics-400, Multi-Moments in Time, and SemanticKITTI. We used a pipeline of existing language models to ground action, object, and relations, filled by manual and automatic curation. We established a comprehensive benchmark for several scenario-based tasks and compared it with

many baseline methods. ScenarioCLIP demonstrates robust zero-shot and finetune performance on various domain-specific tasks. Our code and dataset are available at https://github.com/scenario-clip/ScenarioCLIP.

1. Introduction

To date, the dual stream vision-language pre-training (DSVLPs), which is the general corpus of CLIP-type methods, has widely explored the retrieval of short descriptions or types of objects in the scene. Their popularity stems from strong few-shot and zero-shot performance, in contrast to purely visual models trained with supervised Image-Net-based classification (e.g., AlexNet [27], ResNet [19]). which are typically tied to a fixed label set and must be retrained or finetuned to recognise new categories. To overcome this, the paradigm of DSVLPs decouples the image encoder from the text encoder and extracts features from images and texts simultaneously, leading to simple and flexible adaptations for diverse downstream applications. However, most DSVLPs are restricted to SINGLE-object image classification or short description tasks [13, 32, 48, 69]. A similar limitation holds while using DSVLPs for image retrieval tasks given a text prompt.

However, real-world scenes may contain many objects and actions whose combinations induce complex interobject relations. Prior DSVLP methods mainly improve class separation by: (i) mining harder image-text negatives [47] and (ii) refining text prompts [73], often using LLMs to synthesise or score prompt templates. While these strategies sharpen discrimination over a predefined label set, they operate at the class level and do not explicitly model relations between entities. As a result, embeddings of semantically similar pairs (e.g., person holding bag vs. person holding umbrella) will collapse in representation space.
Among recent advances, PyramidCLIP [14] explores hierarchical alignment by introducing contrastive alignment between global and local features. However. PyramidCLIP

does not explicitly model *inter-object relations* or align features as per relation semantics.

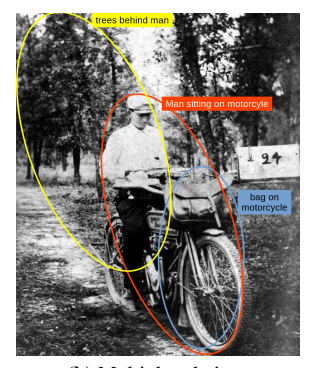
In contrast, the proposed ScenarioCLIP is designed to ingest grounded relational information in scene structure using both the visual and text modalities. On the image side, the model processes the full scene image, the cropped objects and focused regions corresponding to *inter-object relations*. On the text side, the inputs include a global action caption for the scene, object names, and grounded relation descriptions. Each of these streams is encoded by disentangled encoders, allowing us to maintain correspondence between global context (scene/actions) and local evidence (objects and relations). The encoders are initialised with pretrained CLIP [48] weights, providing a strong general-purpose prior that we then specialise to object and relation-level semantics by training on extracted object and focused regions.

As illustrated in Figure 1, real-world scenes typically contain multiple objects and relations that cannot be captured by a single global description and image-level feature. In Figure 1(a), the scene involves a single clearly grounded relation (motorcycle parked on street), which can still be aligned to an appropriate global description by standard CLIP-style models, even though the relation itself remains implicit and unlabeled. In contrast, Figure 1(b) shows a scene with overlapping relations (man sitting on motorcycle, bag on motorcycle, trees behind man), where one global caption cannot specify which objects participate in which interactions or localise these interactions. ScenarioCLIP explicitly addresses this setting by detecting actions and objects and localising the corresponding relations between them, associating each grounded relation text with its focused region (Figure 2).

To model the aforementioned complex scene-based relationship along with the modality-based cross-alignment, ScenarioCLIP incorporates an EMA-based knowledge-distillation within the vision-language space. We maintain an EMA-based teacher of the model and enforce consistency between global scene-level embeddings and their corresponding object and relation-level embeddings in both the visual and textual modalities. This transfer helps to stabilise high-level semantics into local representations without relying on external knowledge graphs or additional VLM teachers, in contrast to Structure-CLIP [21].

Further, to address the lack of large-scale datasets with grounded actions, objects, and relations across diverse scenarios, we also introduce the *Action-Genome Dataset*. This proposed dataset contains approximately 600K images annotated with a global action caption, a list of object names, and multiple relation triplets (object₁, relation, object₂) per image, each linked to object bounding boxes and relation-focused regions (Section 3). We generate these annotations via a three-stage pipeline that combines a





(a) Single relation

(b) Multiple relations

Figure 1. ScenarioCLIP can not only detect actions and objects but also localize the relations between objects in both single-relation (a) and multi-relation (b) scenes.

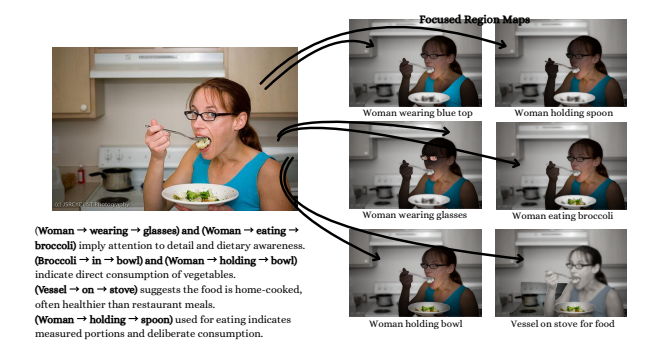
VLM (OpenVLM/Ovis-Gemma [11, 40]) for action, object, and relation text, GroundingDINO [35] for object grounding, and SAM [25] plus RBF-based masking to construct relation-focused regions. In addition, we synthesise hard negative relation triplets via object swaps and antonymbased predicate substitutions, enabling contrastive learning over fine-grained relations. The resulting dataset provides rich supervision for scenario-level scene understanding and fills an important gap for training and evaluating models such as ScenarioCLIP.

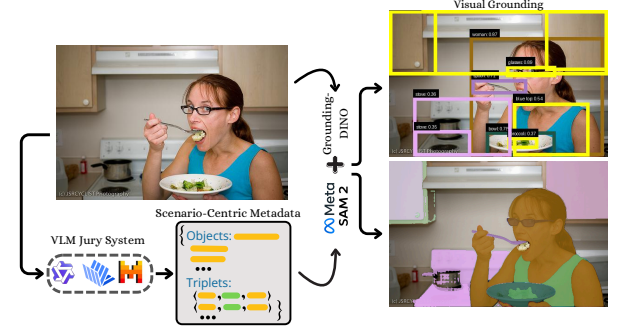
In summary, the contributions of this paper are threefold:

- We introduce ScenarioCLIP, a relation-aware visionlanguage model that jointly encodes global scene context, objects, and inter-object relations within a scene, enabling multi-relation classification and object detection in complex scenes.
- We construct the Action-Genome Dataset, a 600K-image corpus with action, object, and relation annotations, object bounding boxes, and relation-focused regions, providing a new dataset for scene understanding.
- We propose an EMA-based, intra-modal knowledgedistillation objective that refines object- and relation-level representations by enforcing consistency between global scene-level and local embeddings on both image and text branches.

2. Literature

Vision Language Pre-Training (VLP) models have become powerful baselines for various downstream tasks, offering a unified understanding of visual and textual data by aligning vision and language modalities [51, 52, 61, 75]. The pre-training phase has followed two primary strategies: Supervised pre-training, using labeled datasets like ImageNet for feature learning with a supervised loss [7, 16], and unsupervised pre-training for self-supervised learning from unlabeled data [5, 18, 20]. Recent work also leverages large





(a) Scenario-centric annotation pipeline.

Figure 2. Focused regions and scenario-centric grounding. (a) Our pipeline generates relation-focused regions for each triplet (e.g., woman wearing glasses, vessel on stove for food). (b) A VLM produces scenario-centric metadata, which GroundingDINO [35] and SAM [25] then ground with bounding boxes and segmentation masks that we convert into the focused regions used by ScenarioCLIP.

vision-language models to refine noisy web-scale imagetext corpora and train higher quality CLIP-style models [63]. VLP uniquely supports zero-shot predictions but can be optimized for specific tasks through dataset formatting, novel objectives, and high-capacity model designs [69–71].

VLP advances have catalysed two main directions: Transfer Learning, employing prompt tuning and visual adaptation [12, 72-74], and Knowledge Distillation, where pre-trained VLM knowledge transfers to specific tasks like open-vocabulary object detection and segmentation [9, 10, 17]. Beyond these, post-pre-training methods such as CLIP-Refine [66] explicitly reduce the image-text modality gap in CLIP-style models and continual learning frameworks like C-CLIP [36] aim to preserve zero-shot capabilities while adapting to new multimodal tasks. Dual-stream models like CLIP [48], which decouple image and text encoders, dominate VLP due to flexible adaptation and transfer learning [22, 30, 31, 39]. CLIP's contrastive learning over large-scale image-text pairs supports zero-shot capabilities across tasks such as zero-shot classification [26, 50], openvocabulary segmentation [46, 54, 77], human action recognition [42, 59] and out-of-distribution detection [1, 57]. A growing body of models has extended CLIP's architecture to new applications. For scene understanding and detailed focus, PyramidCLIP [14] improves multiscale feature extraction, FocusCLIP [24] and Eyes Wide Shut [55] enhance VQA, and CLIP-Adapter [12] along with Prompt-CLIP [6] support task adaptation through lightweight layers and prompt-based tuning.

In dynamic content, ACTION-CLIP [58] and Video-Composer [60] introduce temporal elements for video analysis and synthesis. Generative models, including CLIP-GEN [62] and BLIP-Diffusion [29], blend contrastive and diffusion-based approaches for text-to-visual generation. For image-to-3D tasks, Wonder3D [37] and One-2-3-45++ [34] incorporate cross-domain techniques, broad-

ening CLIP's impact in 3D reconstruction.

In segmentation and scene understanding, GroupViT [64] enables open-vocabulary segmentation, and VeCLIP [28] enhances visual captioning. Autonomous navigation models like DriveGPT4 [65] leverage CLIP's vision-language outputs for driving tasks. Multimodal instruction advancements, such as Visual Instruction Tuning [33] and MM1 methodology [41], utilize fine-tuning to enhance visual search and multimodal Q&A, showcasing CLIP's adaptability across complex vision-language tasks.

3. Action-Genome Dataset

The Action Genome Dataset consists of approximately 600,000 data points, each structured with multiple layers of descriptive and relational information about actions within visual scenes. At the core of each data point is the original image, representing the primary visual input from which the subsequent annotations and relationships are derived.

Stage 1- VLM: Each image is annotated with a main action label and a concise text caption that describes the primary action occurring within the scene. To complement this action-focused description, each image also includes a list of objects presented as text captions, identifying all visible objects in the scene. The number of objects varies by image, and a single object type may appear multiple times within the same frame, denoting distinct instances. Additionally, to capture spatial and contextual relationships between objects, each image includes a set of relation triplets. Each triplet is structured as $(object_1, relation, object_2)$, where relation indicates a specific interaction or association between $object_1$ and $object_2$. Importantly, each image contains at least three such triplets, offering rich relational data that enables fine-grained understanding of object interactions within the scene. Each triplet contains at least 3 negative triplets, not accurately depicting the scene in focus, which will be used in contrastive learning for understanding the focused region.

Stage 2-Grounding-DINO [35]: For each identified object, the dataset provides precise bounding boxes that define the object's location within the image.

Stage 3- Focused Region - SAM [25]: Furthermore, each relation triplet is supplemented with focused regions, which are specific areas of the image that highlight the spatial context of the respective relation. These regions emphasize the segments of the image where the interaction between *object*₁ and *object*₂ is most pronounced, thereby enhancing the interpretability of the relational data. Together, these components provide a comprehensive, multifaceted view of actions, objects, and relationships within visual scenes, making the Action-Genome Dataset a valuable resource for action recognition and visual relationship detection research.

3.1. Models used for Stage-wise Generation

Stage-1 uses an open-weight VLM (Ovis-Gemma 9B [11, 40]) to generate a global action caption, object list, and relation triplets for each image, based on a custom prompt. Stage-2 applies GroundingDINO [35], prompted with the object list, to predict bounding boxes $(x_{\min}, y_{\min}, x_{\max}, y_{\max})$ for all mentioned objects. Stage-3 uses SAM [25] to obtain object masks and then constructs relation-focused regions by spatially weighting and blending the masks with the original image. Further implementation details (prompt details and the exact RBF/Gaussian weighting used to form focused regions) are provided in the supplementary material.

3.2. Constituent Datasets and Curation

We construct the Action-Genome Dataset from five publicly available sources: OpenPSG [76], Panoptic Video Scene Graph [68], Kinetics-400 [23], Multi-Moments in Time [44], and SemanticKITTI [2, 15]. Wherever available, we reuse ground-truth labels (e.g., action classes in Kinetics-400 and Multi-Moments, and relations in Open-PVSG).

Further, to add onto the existing data, we generate a few negative relations for every focused region, to use for contrastive alignment during the training of the CLIP Model. We generate the negative relation triplets using two methods:

- We swap out the objects that make the relation triplet, which is of the form (object₁, relation, object₂), with a different object from the image, provided the swap doesn't lead to another positive triplet corresponding to a different focused region.
- We use a predefined dictionary of opposites to replace the relation part of the triplet with its opposite. We find the key from the dictionary based on the similarity score of relation with all the keys of the dictionary.

To obtain a clean label space, we normalize and consolidate the raw action, object, and relation vocabularies using a combination of automatic filtering and clustering, as well as manual curation, yielding condensed sets of action, object, and relation classes used in all our experiments. Additional details of this negative sampling and curation are provided in the supplementary material.

Our final Action-Genome Dataset contains **615,805** images, **740** action classes, **4,812** object classes, and **225,609** relation classes.

4. Scenario CLIP Architecture

The ScenarioCLIP architecture consists of three visual encoders $f_{V,G}$, $f_{V,O}$ and $f_{V,R}$ and three text encoders $f_{T,G}$, $f_{T,O}$ and $f_{T,R}$, each dedicated to extracting features at different levels–global, object, and relation respectively from visual and textual inputs derived from the Action-Genome dataset (Figure 4). All encoders are initialized with pretrained CLIP weights (openai/clip-vit-base-patch32 [48]), providing a strong general-purpose vision-language prior that is then specialized for scene-, object-, and relation-level semantics during ScenarioCLIP training. In particular, the object and relation encoders are trained on single-object crops and relation-focused regions, respectively, which specializes them for recognizing objects and relations in holistic scenes.

These multi-level encoders yield six distinct feature representations, which we denote as follows: V_G represents the **Global Visual Embedding**; $V_{O,1}, V_{O,2}, V_{O,3}, \ldots, V_{O,n_O}$ denote the **Object Visual Embeddings**; and $V_{R,1}, V_{R,2}, V_{R,3}, \ldots, V_{R,n_R}$ represent the **Relation Visual Embeddings**. Similarly, we define T_G as the **Global Text Embedding**; $T_{O,1}, T_{O,2}, T_{O,3}, \ldots, T_{O,n_O}$ as the **Object Text Embeddings**; and $T_{R,1}, T_{R,2}, T_{R,3}, \ldots, T_{R,n_R}$ as the **Relation Text Embeddings**. The embedding sizes of V_G and T_G are 12, of 120 are 131 and 132 are 133 are 134 and 135 are 135 and 136 are 137 and 138 are 139 and 139 are 139 are 139 and 139 are 139 and 139 are 139 are 139 and 139 are 139 are 139 are 139 are 139 and 139 are 139 are

4.1. Knowledge Distillation

An Exponential-Moving Average (EMA)-based Knowledge distillation serves as a logical enhancement to the architecture by facilitating the transfer of high-level, comprehensive representations between the global embeddings and the more granular embeddings at the object and relation levels. The EMA-updated teacher provides temporally smoothed targets, lower-variance targets that offer structured guidance to the student. In multi-level architectures such as ScenarioCLIP, global embeddings (such as V_G and T_G) inherently capture a broader, context-enriched understanding of the scene, providing a coherent overview that complements the finer, specific details encoded in the object and rela-

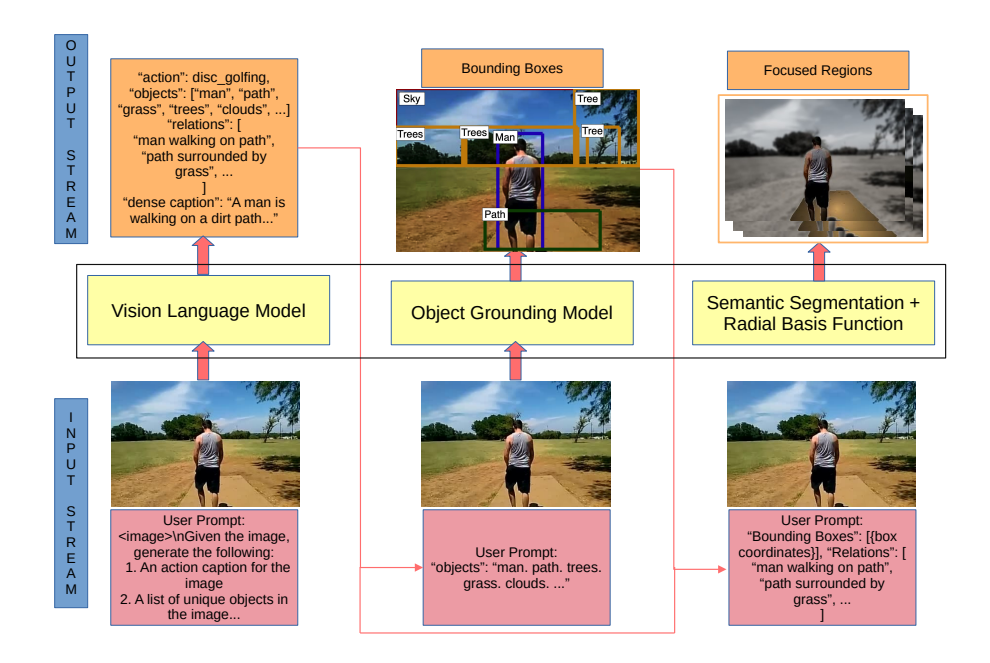


Figure 3. Data generation pipeline for the Action-Genome Dataset. Given a raw image, a vision-language model produces a global action caption, object list, and relation triplets (left). An object grounding model (GroundingDINO [35]) then predicts bounding boxes for the mentioned objects (middle). Finally, a segmentation model (SAM [25]) with RBF-based weighting constructs relation-focused regions that highlight the spatial context of each (object₁, relation, object₂) triplet (right).

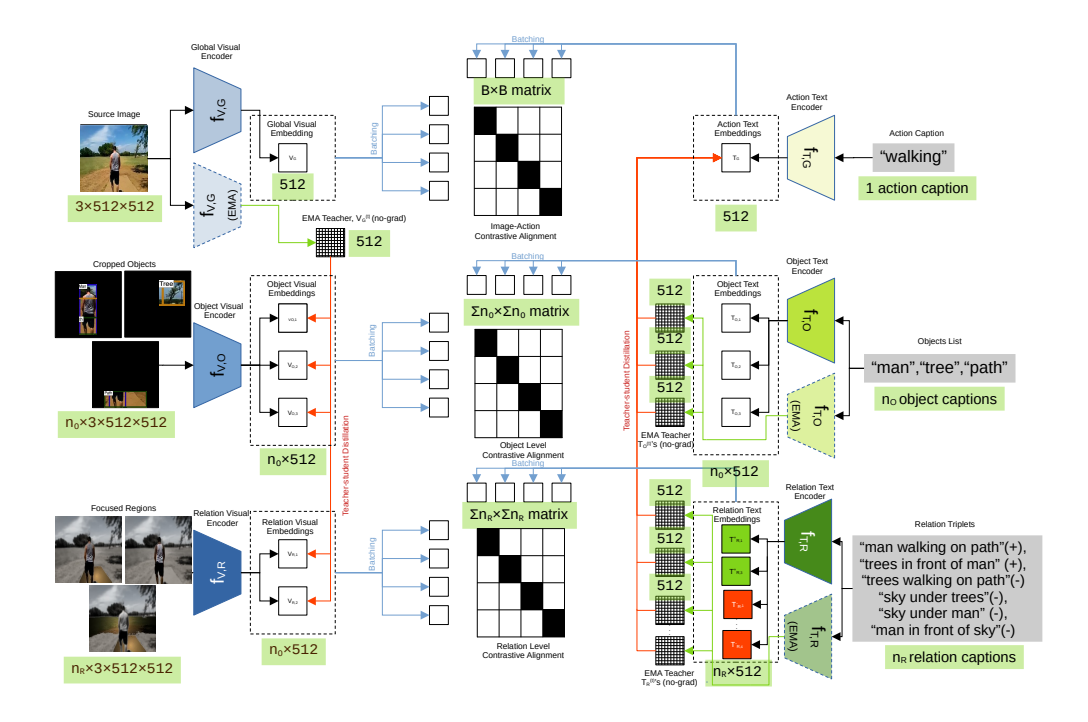


Figure 4. Overview of ScenarioCLIP. A global, object, and relation encoder extracts visual features from the full image, object crops, and focused regions, while corresponding text encoders embed the action caption, object names, and relation triplets. Contrastive losses align image-action, object-object, and relation-relation pairs, and EMA teachers provide knowledge-distillation targets.

tion embeddings ($V_{O,i}$, $V_{R,i}$). By distilling knowledge from these global embeddings to their respective lower-level embeddings, the architecture benefits from a structured guidance mechanism. This process not only helps the network maintain a consistent interpretation across hierarchical levels but also enables the model to learn more robust representations with improved generalization. The use of Kullback-Leibler (KL) divergence within this EMA-based distillation enforces a smoothh mutual alignment between embeddings, promoting synergy between the high-level overview and the detailed components, thus improving the performance of the model in tasks that require both contextual understanding and precise relational reasoning.

At each training step, the EMA teacher network is updated as a slow-moving average of the student parameters, providing stable, non-noisy targets for the distillation. For the visual modality, we transfer knowledge from the EMA teacher $V_G^{(t)}$, which is expected to capture a higher degree of global information, to each object-level embedding $V_{O,i}$ and each relation-level embedding $V_{R,i}$. This is accomplished by creating a cloned, frozen version of $V_G^{(t)}$, which is detached from the computational graph. We then use Kullback-Leibler (KL) divergence from $V_G^{(t)}$ to each $V_{O,i}$ and $V_{R,i}$ to perform the distillation.

On the text side, the direction of distillation is inverted: we treat each EMA-based object-level embedding $T_{O,i}^{\ (t)}$ and relation-level embedding $T_{R,i}^{\ (t)}$ as a teacher for the global text embedding T_G . This reversal in direction is due to the fact that the fine-grained textual cues about objects and relations collectively define the semantics of the overall scene. Here too, we use cloned, frozen versions of the teacher embeddings, from which we calculate the KL divergence to the global text embedding T_G .

4.2. Contrastive Alignment

To achieve cross-modal alignment, we apply contrastive loss to each corresponding level of visual and text embeddings. This involves calculating contrastive loss between batches of V_G and T_G , batches of $V_{O,i}$ and $T_{O,i}$, and batches of $V_{R,i}$ and $T_{R,i}$. At the relation level alignment, the negative relation triplets for each focused region are used as pseudo labels for better contrastive learning, as demonstrated in [43]. This multi-level alignment promotes coherence across the visual and textual representations at the global, object, and relation levels, enhancing the model's understanding of cross-modal correspondences. The alignment matrix sizes at the global, object and relation level are respectively $B \times B$, $\sum^B n_O \times \sum^B n_O$ and $\sum^B n_R \times \sum^B n_R$.

The use of contrastive alignment in the architecture leverages the fundamental principle of bringing similar representations closer while pushing dissimilar ones apart, thereby aligning visual and textual features at correspond-

ing levels. In the context of ScenarioCLIP, contrastive alignment between visual and text embeddings such as V_G with T_G , $V_{O,i}$ with $T_{O,i}$, and $V_{R,i}$ with $T_{R,i}$ ensures that the representations at each level encode complementary information across modalities. This alignment is crucial for bridging the semantic gap between the visual and textual domains, as it reinforces the model's ability to capture both the distinct characteristics and shared semantics within corresponding global, object, and relation features. By applying contrastive loss across batches, the model learns to associate each level of visual embeddings directly with its textual counterpart, encouraging a one-to-one correspondence between visual and linguistic interpretations of the same concept. This structured alignment not only improves the consistency of cross-modal representations but also enhances the model's capability in tasks that demand finegrained, multi-level understanding across modalities, such as action recognition and relationship detection.

4.3. Objective Function

To combine both knowledge distillation and contrastive alignment, we define an objective function \mathcal{L}_{total} that incorporates both the knowledge distillation loss \mathcal{L}_{KD} and the contrastive alignment loss \mathcal{L}_{CA} . The total loss function can be expressed as:

$$\mathcal{L}_{total} = \lambda_{KD} \cdot \mathcal{L}_{KD} + \lambda_{CA} \cdot \mathcal{L}_{CA} \tag{1}$$

where λ_{KD} and λ_{CA} are weighting coefficients that balance the contributions of the knowledge distillation and contrastive alignment losses, respectively.

The knowledge distillation loss \mathcal{L}_{KD} consists of KL divergence terms that align the global embeddings with the object and relation embeddings within each modality (visual and text). It can be formulated as:

$$\mathcal{L}_{KD} = \sum_{i=1}^{n_O} D_{KL}(V_G || V_{O,i}) + \sum_{j=1}^{n_R} D_{KL}(V_G || V_{R,j}) + \sum_{i=1}^{n_O} D_{KL}(T_{O,i} || T_G) + \sum_{j=1}^{n_R} D_{KL}(T_{R,j} || T_G)$$
 (2)

where $D_{KL}(\cdot \| \cdot)$ denotes the Kullback-Leibler divergence between pairs of embeddings within each modality.

The contrastive alignment loss \mathcal{L}_{CA} encourages alignment between corresponding visual and textual embeddings across levels (global, object, and relation). It can be written as:

$$\mathcal{L}_{CA} = \text{Contrastive}(V_G, T_G) + \sum_{i=1}^{n_O} \text{Contrastive}(V_{O,i}, T_{O,i}) + \sum_{j=1}^{n_R} \text{Contrastive}(V_{R,j}, T_{R,j}) \quad (3)$$

	Actions			Objects			Relations		
Model	Top-1	Top-5	Top-10	Top-1	Top-5	Top-10	Top-1	Top-5	Top-10
A. Ours (in-domain pres	training	on Actic	n-Genom	e Datas	et)				
PyramidCLIP [14]	54.95	73.36	78.84	37.67	59.58	65.92	16.43	34.27	44.20
ScenarioCLIP w/o KD	57.52	75.24	80.34	51.26	64.37	68.32	19.45	36.94	45.75
ScenarioCLIP	57.63	75.02	79.99	51.86	64.43	68.30	19.56	37.03	45.86
B. SoTA zero-shot baselines (released weights; prompt-only)									
CLIP [48]	14.87	33.43	42.45	3.77	12.35	18.39	0.66	2.67	4.72
SLIP [45]	8.31	21.83	30.26	2.96	9.60	14.22	0.35	1.63	3.06

Table 1. Zero-shot (ZS) image→text retrieval on Action-Genome Dataset.

	Actions			Objects			Relations		
Model	Top-1	Top-5	Top-10	Top-1	Top-5	Top-10	Top-1	Top-5	Top-10
PyramidCLIP [14]	75.36	90.54	93.52	79.74	91.79	94.37	40.78	59.73	66.09
ScenarioCLIP w/o KD	79.46	92.94	95.18	84.25	92.38	94.25	44.75	61.02	66.86
ScenarioCLIP	79.19	92.81	95.10	84.30	92.31	94.24	44.71	61.09	66.88

Table 2. Linear-probe results on Action-Genome Dataset.

where Contrastive (\cdot, \cdot) , represents the contrastive loss function applied between corresponding visual and text embeddings at each level. We use the symmetric image-text contrastive object of CLIP with a learnable temperature, following [48].

In summary, the total objective function \mathcal{L}_{total} combines both intra-modality alignment through knowledge distillation and inter-modality alignment through contrastive alignment, facilitating a cohesive learning process that enhances both hierarchical consistency and cross-modal understanding.

5. Experiments

5.1. Implementation Details

Pre-training Stage The models are pretrained on the Action-Genome Dataset introduced in Section 3. We use an AdamW [38] optimizer and a scheduler that applies a linear warm-up over the first 10% of steps, followed by a cosine annealing schedule. For ScenarioCLIP, the distillation temperature is optimized with one-tenth the base learning rate for stability, and the teacher is an EMA of the student with a decay of 0.9995 and a 2000-step warm-up. Additional details are provided in the supplementary material.

Downstream Tasks We evaluate our model on the following downstream tasks: zero-shot image→text retrieval, linear probe, and object detection. All experiments are carried out on the test set of the proposed Action-Genome Dataset.

5.2. Zero-Shot Retrieval

Given an image as a query, we rank a fixed set of class strings using cosine similarity between l2-normalized image and text embeddings, with no task specific tuning of the model. In Table 1A we report in-domain (train and test on Action-Genome Dataset) zero-shot results. ScenarioCLIP outperforms PyramidCLIP [14] across all levels, with the largest gains on *Objects*: 14.19%/4.85%/2.38%on Top-1/5/10 accuracy. We also see a consistent improvement in Actions of 2.68%/1.66%/1.15% and in Relations of 3.13%/2.76%/1.66% over PyramidCLIP [14]. Table 1B shows the zero-shot retrieval results for the publicly available checkpoints of CLIP [48] and SLIP [45]. Prompt templates are used to convert label names into natural-language phrases that better match the pretraining distribution of these models; we average text embeddings over multiple templates for robustness. ScenarioCLIP significantly outperforms these SoTA approaches. Additional details of the prompt templates used are given in the supplementary material.

5.3. Linear-Probe

We freeze the entire model and train task-specific linear heads to predict the action, object, or relation for the given image. The models are fine-tuned for 6 epochs. Table 2 shows that the proposed Scenario-CLIP model significantly outperforms PyramidCLIP [14], with an improvement of 3.83%/4.56%/3.93% on Top-1 *Actions/Objects/Relations*, respectively. This indicates greater class separation in ScenarioCLIP's representation space, with tighter intra-class clusters and larger inter-class

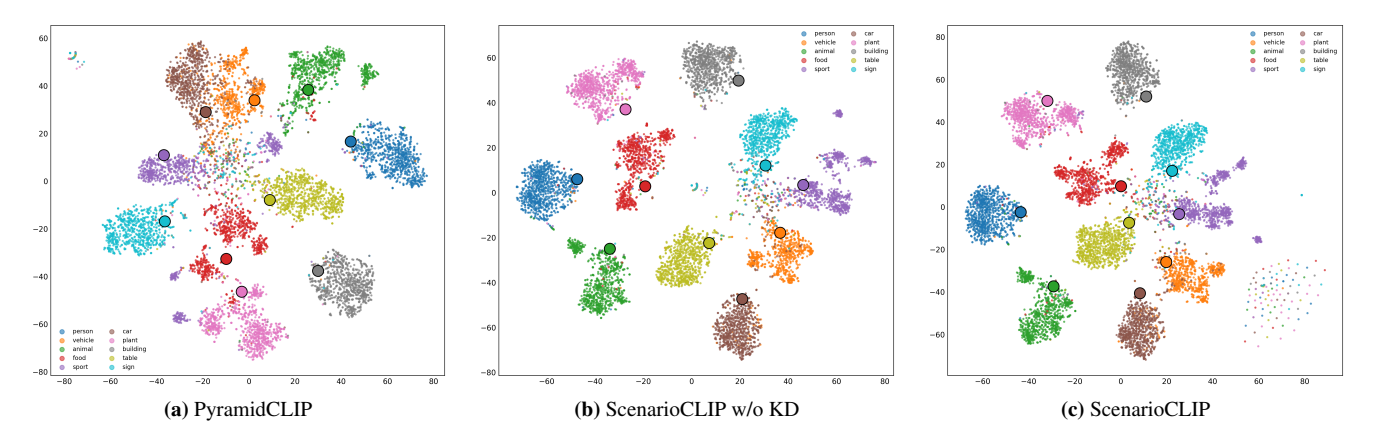


Figure 5. t-SNE visualization of object-level semantic embeddings of 10,000 objects from the Action Genome Dataset. The large points represent the text features and the smaller points represent the image features.

Model	AP^{bb}	AP_{50}^{bb}	AP_{75}^{bb}
PyramidCLIP [14]	9.7	18.6	8.9
ScenarioCLIP w/o KD	9.9	18.7	9.1
ScenarioCLIP	9.9	18.9	9.1

Table 3. Object detection results on the Action-Genome Dataset.

margins than PyramidCLIP [14].

5.4. Object Detection

To evaluate whether improved relational modeling transfers beyond retrieval, we perform object detection, where scene context and object-object interactions are critical. For this, we adopt a Faster R-CNN head and plug our encoders as backbones: for PyramidCLIP [14], the single entangled visual encoder feeds both the RPN and the RoI heads, while for ScenarioCLIP, the global visual encoder provides the RPN features (proposal generation) and the object visual encoder supplies RoI features (classification/regression). This model is trained for 10 epochs on the Action-Genome Dataset. The long-tailed nature of the dataset (4812 object classes) makes object detection a challenging task. ScenarioCLIP yields consistent gains over PyramidCLIP: AP^{bb} improves from 9.7 to 9.9, AP_{50}^{bb} from 18.6 to 18.9, and AP_{75}^{bb} from 8.9 to 9.1 (Table 3). These improvements highlight ScenarioCLIP's stronger object-aware representations and effectiveness in preserving fine-grained spatial information.

5.5. Ablation Study

To isolate the contribution of the knowledge distillation objective, we perform experiments without the KD objective. Table 1 shows that the KD objective provides gains in zero-shot image \rightarrow text retrieval, particularly for *Objects* with an improvement of 0.6% over ScenarioCLIP without

KD. The global-local KD objective also helps in object detection (Table 3), with an improvement of 0.2 in AP_{50}^{bb} . We attribute this to improved representation learning from the EMA knowledge distillation. The linear-probe results in Table 2 show marginal differences between the two models. These results suggest that KD refines the structure of the embedding space to generalize better to unseen classes, while preserving comparable linear classification capacity.

5.6. Visualizations

To qualitatively assess the learned representation space, we visualize the object-level semantic embeddings of 10,000 objects from the test and validation set of the Action Genome Dataset using t-SNE [56] (Figure 5). In Pyramid-CLIP [14], the clusters are overlapping and loosely formed. ScenarioCLIP w/o KD shows clearer separation between categories, but the clusters remain relatively sparse. In contrast, ScenarioCLIP produces compact and well-organized clusters with minimal overlap, with similar categories like (car, vehicle) being close together. This demonstrates that the proposed intra-modal knowledge distillation enhances both feature compactness and semantic alignment.

6. Conclusion

In this paper, we have proposed a relation-aware vision-language pretraining framework, called *ScenarioCLIP*, to explicitly model actions, objects, and grounded inter-object relations in complex scenes. Built on disentangled global, object, and relation encoders with an EMA-based knowledge-distillation objective, ScenarioCLIP achieves improved cross-modal alignment at both scene and relation levels. We further introduce the *Action-Genome Dataset*, a large-scale corpus with action captions, object labels, relation triplets, and relation-focused regions to support scenario-level training and evaluation. Extensive experiments on zero-shot retrieval, linear-probe, and object de-

tection demonstrate the effectiveness and superiority of our approach.

References

- [1] Nikolas Adaloglou, Felix Michels, Tim Kaiser, and Markus Kollmann. Adapting contrastive language-image pretrained (clip) models for out-of-distribution detection, 2023. 3
- [2] J. Behley, M. Garbade, A. Milioto, J. Quenzel, S. Behnke, C. Stachniss, and J. Gall. SemanticKITTI: A Dataset for Semantic Scene Understanding of LiDAR Sequences. In *Proc.* of the IEEE/CVF International Conf. on Computer Vision (ICCV), 2019. 4
- [3] Steven Bird, Ewan Klein, and Edward Loper. *Natural language processing with Python: analyzing text with the natural language toolkit.* "O'Reilly Media, Inc.", 2009. 1
- [4] Ricardo J. G. B. Campello, Davoud Moulavi, and Joerg Sander. Density-based clustering based on hierarchical density estimates. In *Advances in Knowledge Discovery and Data Mining*, pages 160–172, Berlin, Heidelberg, 2013. Springer Berlin Heidelberg. 1
- [5] Ting Chen, Simon Kornblith, Mohammad Norouzi, and Geoffrey Hinton. A simple framework for contrastive learning of visual representations, 2020. 2
- [6] Weiwen Chen, Qiuhong Ke, and Zinuo Li. Clip guided image-perceptive prompt learning for image enhancement, 2023. 3
- [7] Jia Deng, Wei Dong, Richard Socher, Li-Jia Li, Kai Li, and Li Fei-Fei. Imagenet: A large-scale hierarchical image database. In 2009 IEEE conference on computer vision and pattern recognition, pages 248–255. Ieee, 2009. 2
- [8] Jacob Devlin, Ming-Wei Chang, Kenton Lee, and Kristina Toutanova. Bert: Pre-training of deep bidirectional transformers for language understanding, 2019.
- [9] Jian Ding, Nan Xue, Gui-Song Xia, and Dengxin Dai. Decoupling zero-shot semantic segmentation, 2022. 3
- [10] Yu Du, Fangyun Wei, Zihe Zhang, Miaojing Shi, Yue Gao, and Guoqi Li. Learning to prompt for open-vocabulary object detection with vision-language model, 2022. 3
- [11] Gemma Team et al. Gemma 2: Improving open language models at a practical size, 2024. 2, 4, 1
- [12] Peng Gao, Shijie Geng, Renrui Zhang, Teli Ma, Rongyao Fang, Yongfeng Zhang, Hongsheng Li, and Yu Qiao. Clip-adapter: Better vision-language models with feature adapters, 2021. 3
- [13] Yuting Gao, Jinfeng Liu, Zihan Xu, Jun Zhang, Ke Li, Rongrong Ji, and Chunhua Shen. Pyramidelip: Hierarchical feature alignment for vision-language model pretraining. Advances in neural information processing systems, 35:35959–35970, 2022. 1
- [14] Yuting Gao, Jinfeng Liu, Zihan Xu, Jun Zhang, Ke Li, Rongrong Ji, and Chunhua Shen. Pyramidclip: Hierarchical feature alignment for vision-language model pretraining, 2022. 1, 3, 7, 8, 2, 4, 5
- [15] A. Geiger, P. Lenz, and R. Urtasun. Are we ready for Autonomous Driving? The KITTI Vision Benchmark Suite. In *Proc. of the IEEE Conf. on Computer Vision and Pattern Recognition (CVPR)*, pages 3354–3361, 2012. 4

- [16] Ross Girshick. Fast r-cnn, 2015. 2
- [17] Xiuye Gu, Tsung-Yi Lin, Weicheng Kuo, and Yin Cui. Open-vocabulary object detection via vision and language knowledge distillation, 2022. 3
- [18] Jie Gui, Tuo Chen, Jing Zhang, Qiong Cao, Zhenan Sun, Hao Luo, and Dacheng Tao. A survey on self-supervised learning: Algorithms, applications, and future trends, 2024.
- [19] Kaiming He, Xiangyu Zhang, Shaoqing Ren, and Jian Sun. Deep residual learning for image recognition, 2015. 1
- [20] Kaiming He, Haoqi Fan, Yuxin Wu, Saining Xie, and Ross Girshick. Momentum contrast for unsupervised visual representation learning, 2020. 2
- [21] Yufeng Huang, Jiji Tang, Zhuo Chen, Rongsheng Zhang, Xinfeng Zhang, Weijie Chen, Zeng Zhao, Zhou Zhao, Tangjie Lv, Zhipeng Hu, and Wen Zhang. Structure-clip: Towards scene graph knowledge to enhance multi-modal structured representations, 2023.
- [22] Chao Jia, Yinfei Yang, Ye Xia, Yi-Ting Chen, Zarana Parekh, Hieu Pham, Quoc V. Le, Yunhsuan Sung, Zhen Li, and Tom Duerig. Scaling up visual and vision-language representation learning with noisy text supervision, 2021. 3
- [23] Will Kay, Joao Carreira, Karen Simonyan, Brian Zhang, Chloe Hillier, Sudheendra Vijayanarasimhan, Fabio Viola, Tim Green, Trevor Back, Paul Natsev, Mustafa Suleyman, and Andrew Zisserman. The kinetics human action video dataset, 2017. 4
- [24] Muhammad Saif Ullah Khan, Muhammad Ferjad Naeem, Federico Tombari, Luc Van Gool, Didier Stricker, and Muhammad Zeshan Afzal. Human pose descriptions and subject-focused attention for improved zero-shot transfer in human-centric classification tasks, 2024. 3
- [25] Alexander Kirillov, Eric Mintun, Nikhila Ravi, Hanzi Mao, Chloe Rolland, Laura Gustafson, Tete Xiao, Spencer Whitehead, Alexander C. Berg, Wan-Yen Lo, Piotr Dollár, and Ross Girshick. Segment anything, 2023. 2, 3, 4, 5, 1
- [26] Alex Krizhevsky. Learning multiple layers of features from tiny images. pages 32–33, 2009. 3
- [27] Alex Krizhevsky, Ilya Sutskever, and Geoffrey E. Hinton. Imagenet classification with deep convolutional neural networks. In *Proceedings of the 26th International Conference* on Neural Information Processing Systems - Volume 1, page 1097–1105, Red Hook, NY, USA, 2012. Curran Associates Inc. 1
- [28] Zhengfeng Lai, Haotian Zhang, Bowen Zhang, Wentao Wu, Haoping Bai, Aleksei Timofeev, Xianzhi Du, Zhe Gan, Jiulong Shan, Chen-Nee Chuah, Yinfei Yang, and Meng Cao. Veclip: Improving clip training via visual-enriched captions, 2024. 3
- [29] Dongxu Li, Junnan Li, and Steven C. H. Hoi. Blip-diffusion: Pre-trained subject representation for controllable text-toimage generation and editing, 2023. 3
- [30] Gen Li, Nan Duan, Yuejian Fang, Ming Gong, Daxin Jiang, and Ming Zhou. Unicoder-vl: A universal encoder for vision and language by cross-modal pre-training, 2019. 3
- [31] Liunian Harold Li, Mark Yatskar, Da Yin, Cho-Jui Hsieh, and Kai-Wei Chang. Visualbert: A simple and performant baseline for vision and language, 2019. 3

- [32] Yangguang Li, Feng Liang, Lichen Zhao, Yufeng Cui, Wanli Ouyang, Jing Shao, Fengwei Yu, and Junjie Yan. Supervision exists everywhere: A data efficient contrastive language-image pre-training paradigm, 2022.
- [33] Haotian Liu, Chunyuan Li, Qingyang Wu, and Yong Jae Lee. Visual instruction tuning, 2023. 3
- [34] Minghua Liu, Ruoxi Shi, Linghao Chen, Zhuoyang Zhang, Chao Xu, Xinyue Wei, Hansheng Chen, Chong Zeng, Jiayuan Gu, and Hao Su. One-2-3-45++: Fast single image to 3d objects with consistent multi-view generation and 3d diffusion, 2023. 3
- [35] Shilong Liu, Zhaoyang Zeng, Tianhe Ren, Feng Li, Hao Zhang, Jie Yang, Chunyuan Li, Jianwei Yang, Hang Su, Jun Zhu, et al. Grounding dino: Marrying dino with grounded pre-training for open-set object detection. *arXiv preprint arXiv:2303.05499*, 2023. 2, 3, 4, 5, 1
- [36] Wenzhuo Liu, Fei Zhu, Longhui Wei, and Qi Tian. C-CLIP: Multimodal continual learning for vision-language model. In The Thirteenth International Conference on Learning Representations, 2025. 3
- [37] Xiaoxiao Long, Yuan-Chen Guo, Cheng Lin, Yuan Liu, Zhiyang Dou, Lingjie Liu, Yuexin Ma, Song-Hai Zhang, Marc Habermann, Christian Theobalt, and Wenping Wang. Wonder3d: Single image to 3d using cross-domain diffusion, 2023. 3
- [38] Ilya Loshchilov and Frank Hutter. Decoupled weight decay regularization, 2019. 7, 2, 3
- [39] Jiasen Lu, Dhruv Batra, Devi Parikh, and Stefan Lee. Vilbert: Pretraining task-agnostic visiolinguistic representations for vision-and-language tasks, 2019. 3
- [40] Shiyin Lu, Yang Li, Qing-Guo Chen, Zhao Xu, Weihua Luo, Kaifu Zhang, and Han-Jia Ye. Ovis: Structural embedding alignment for multimodal large language model. arXiv:2405.20797, 2024. 2, 4, 1
- [41] Brandon McKinzie, Zhe Gan, Jean-Philippe Fauconnier, Sam Dodge, Bowen Zhang, Philipp Dufter, Dhruti Shah, Xianzhi Du, Futang Peng, Floris Weers, Anton Belyi, Haotian Zhang, Karanjeet Singh, Doug Kang, Ankur Jain, Hongyu Hè, Max Schwarzer, Tom Gunter, Xiang Kong, Aonan Zhang, Jianyu Wang, Chong Wang, Nan Du, Tao Lei, Sam Wiseman, Guoli Yin, Mark Lee, Zirui Wang, Ruoming Pang, Peter Grasch, Alexander Toshev, and Yinfei Yang. Mm1: Methods, analysis & insights from multimodal llm pretraining, 2024. 3
- [42] Antoine Miech, Jean-Baptiste Alayrac, Ivan Laptev, Josef Sivic, and Andrew Zisserman. Rareact: A video dataset of unusual interactions, 2020. 3
- [43] Sangwoo Mo, Minkyu Kim, Kyungmin Lee, and Jinwoo Shin. S-CLIP: Semi-supervised vision-language learning using few specialist captions. In *Thirty-seventh Conference on Neural Information Processing Systems*, 2023. 6
- [44] Mathew Monfort, Bowen Pan, Kandan Ramakrishnan, Alex Andonian, Barry A McNamara, Alex Lascelles, Quanfu Fan, Dan Gutfreund, Rogerio Feris, and Aude Oliva. Multimoments in time: Learning and interpreting models for multi-action video understanding, 2021. 4

- [45] Norman Mu, Alexander Kirillov, David Wagner, and Saining Xie. Slip: Self-supervision meets language-image pretraining, 2021. 7
- [46] Zelin Peng, Zhengqin Xu, Changsong Wen, Yu Huang, Menglin Yang, Feilong Tang, and Wei Shen. Understanding fine-tuning CLIP for open-vocabulary semantic segmentation in hyperbolic space. In 2nd Beyond Euclidean Workshop: Hyperbolic and Hyperspherical Learning for Computer Vision, 2025. 3
- [47] Filip Radenovic, Abhimanyu Dubey, Abhishek Kadian, Todor Mihaylov, Simon Vandenhende, Yash Patel, Yi Wen, Vignesh Ramanathan, and Dhruv Mahajan. Filtering, distillation, and hard negatives for vision-language pre-training, 2023. 1
- [48] Alec Radford, Jong Wook Kim, Chris Hallacy, Aditya Ramesh, Gabriel Goh, Sandhini Agarwal, Girish Sastry, Amanda Askell, Pamela Mishkin, Jack Clark, Gretchen Krueger, and Ilya Sutskever. Learning transferable visual models from natural language supervision, 2021. 1, 2, 3, 4, 7
- [49] Shaoqing Ren, Kaiming He, Ross Girshick, and Jian Sun. Faster r-cnn: Towards real-time object detection with region proposal networks, 2016. 3
- [50] Fawaz Sammani and Nikos Deligiannis. Interpreting and analyzing clip's zero-shot image classification via mutual knowledge, 2024. 3
- [51] Christoph Schuhmann, Richard Vencu, Romain Beaumont, Robert Kaczmarczyk, Clayton Mullis, Aarush Katta, Theo Coombes, Jenia Jitsev, and Aran Komatsuzaki. Laion-400m: Open dataset of clip-filtered 400 million image-text pairs, 2021. 2
- [52] Christoph Schuhmann, Romain Beaumont, Richard Vencu, Cade Gordon, Ross Wightman, Mehdi Cherti, Theo Coombes, Aarush Katta, Clayton Mullis, Mitchell Wortsman, Patrick Schramowski, Srivatsa Kundurthy, Katherine Crowson, Ludwig Schmidt, Robert Kaczmarczyk, and Jenia Jitsev. Laion-5b: An open large-scale dataset for training next generation image-text models, 2022. 2
- [53] Ramprasaath R. Selvaraju, Michael Cogswell, Abhishek Das, Ramakrishna Vedantam, Devi Parikh, and Dhruv Batra. Grad-cam: Visual explanations from deep networks via gradient-based localization. *International Journal of Com*puter Vision, 128(2):336–359, 2019. 4, 5
- [54] Tong Shao, Zhuotao Tian, Hang Zhao, and Jingyong Su. Explore the potential of clip for training-free open vocabulary semantic segmentation, 2024. 3
- [55] Shengbang Tong, Zhuang Liu, Yuexiang Zhai, Yi Ma, Yann LeCun, and Saining Xie. Eyes wide shut? exploring the visual shortcomings of multimodal llms, 2024. 3
- [56] Laurens van der Maaten, Geoffrey Hinton, and Yoesoep Rachmad. Viualizing data using t-sne. *Journal of Machine Learning Research*, 9:2579–2605, 2008.
- [57] Hualiang Wang, Yi Li, Huifeng Yao, and Xiaomeng Li. Clipn for zero-shot ood detection: Teaching clip to say no, 2023. 3
- [58] Mengmeng Wang, Jiazheng Xing, and Yong Liu. Actionclip: A new paradigm for video action recognition, 2021. 3

- [59] Qiang Wang, Junlong Du, Ke Yan, and Shouhong Ding. Seeing in flowing: Adapting clip for action recognition with motion prompts learning, 2023. 3
- [60] Xiang Wang, Hangjie Yuan, Shiwei Zhang, Dayou Chen, Jiuniu Wang, Yingya Zhang, Yujun Shen, Deli Zhao, and Jingren Zhou. Videocomposer: Compositional video synthesis with motion controllability, 2023. 3
- [61] Xiyao Wang, Jiuhai Chen, Zhaoyang Wang, Yuhang Zhou, Yiyang Zhou, Huaxiu Yao, Tianyi Zhou, Tom Goldstein, Parminder Bhatia, Furong Huang, and Cao Xiao. Enhancing visual-language modality alignment in large vision language models via self-improvement, 2024. 2
- [62] Zihao Wang, Wei Liu, Qian He, Xinglong Wu, and Zili Yi. Clip-gen: Language-free training of a text-to-image generator with clip, 2022. 3
- [63] Zhixiang Wei, Guangting Wang, Xiaoxiao Ma, Ke Mei, Huaian Chen, Yi Jin, and Fengyun Rao. Hq-clip: Leveraging large vision-language models to create high-quality imagetext datasets and clip models, 2025. 3
- [64] Jiarui Xu, Shalini De Mello, Sifei Liu, Wonmin Byeon, Thomas Breuel, Jan Kautz, and Xiaolong Wang. Groupvit: Semantic segmentation emerges from text supervision, 2022.
- [65] Zhenhua Xu, Yujia Zhang, Enze Xie, Zhen Zhao, Yong Guo, Kwan-Yee. K. Wong, Zhenguo Li, and Hengshuang Zhao. Drivegpt4: Interpretable end-to-end autonomous driving via large language model, 2024. 3
- [66] Shin'ya Yamaguchi, Dewei Feng, Sekitoshi Kanai, Kazuki Adachi, and Daiki Chijiwa. Post-pre-training for modality alignment in vision-language foundation models, 2025. 3
- [67] Burhaneddin Yaman, Tanvir Mahmud, and Chun-Hao Liu. Instance-aware repeat factor sampling for long-tailed object detection, 2023. 3
- [68] Jingkang Yang, Wenxuan Peng, Xiangtai Li, Zujin Guo, Liangyu Chen, Bo Li, Zheng Ma, Kaiyang Zhou, Wayne Zhang, Chen Change Loy, and Ziwei Liu. Panoptic video scene graph generation, 2023. 4
- [69] Lewei Yao, Runhui Huang, Lu Hou, Guansong Lu, Minzhe Niu, Hang Xu, Xiaodan Liang, Zhenguo Li, Xin Jiang, and Chunjing Xu. Filip: Fine-grained interactive language-image pre-training, 2021. 1, 3
- [70] Jiahui Yu, Zirui Wang, Vijay Vasudevan, Legg Yeung, Mojtaba Seyedhosseini, and Yonghui Wu. Coca: Contrastive captioners are image-text foundation models, 2022.
- [71] Jingyi Zhang, Jiaxing Huang, Sheng Jin, and Shijian Lu. Vision-language models for vision tasks: A survey, 2024.
- [72] Renrui Zhang, Rongyao Fang, Wei Zhang, Peng Gao, Kunchang Li, Jifeng Dai, Yu Qiao, and Hongsheng Li. Tip-adapter: Training-free clip-adapter for better visionlanguage modeling, 2021. 3
- [73] Kaiyang Zhou, Jingkang Yang, Chen Change Loy, and Ziwei Liu. Learning to prompt for vision-language models. *International Journal of Computer Vision*, 130(9):2337–2348, 2022.
- [74] Kaiyang Zhou, Jingkang Yang, Chen Change Loy, and Ziwei Liu. Conditional prompt learning for vision-language models, 2022. 3

- [75] Yiyang Zhou, Chenhang Cui, Rafael Rafailov, Chelsea Finn, and Huaxiu Yao. Aligning modalities in vision large language models via preference fine-tuning, 2024. 2
- [76] Zijian Zhou, Zheng Zhu, Holger Caesar, and Miaojing Shi. Openpsg: Open-set panoptic scene graph generation via large multimodal models, 2024. 4
- [77] Wenqi Zhu, Jiale Cao, Jin Xie, Shuangming Yang, and Yan-wei Pang. Clip-vis: Adapting clip for open-vocabulary video instance segmentation, 2024. 3

ScenarioCLIP: Pretrained Transferable Visual Language Models and Action-Genome Dataset for Natural Scene Analysis

Supplementary Material

7. Models used for Stage-wise Dataset Generation

Stage-1 of our generation pipeline involves using an OpenVLM(Ovis-Gemma 9B [11, 40]). This model generates annotations based on a carefully crafted custom prompt. We experimented with different phrasing structures, adjusting syntax. These experiments were crucial in impacting the quality of our final annotations.

In Stage-2, we use the GroundingDINO [35] model , for retrieving the bounding boxes. GroundingDINO is prompted with a fullstop-separated list of objects as a single string, to return the bounding box coordinates as $(x_{\min}, y_{\min}, x_{\max}, y_{\max})$

Stage-3 of our generation pipeline, which involves generating focused regions, first generates the segmentation masks of each object, detected by GroundingDINO using the Segment Anything Model(SAM) [25]. These segmentation masks are used to construct focused regions using a combination of mathematical functions applied to the image.

By leveraging Radial Basis Functions centered on the objects' centers of mass, we create masks that highlight spatial interactions based on distance, effectively blending these masks with the original images.

$$RBF(\mathbf{x}) = e^{-\frac{\|\mathbf{x} - \mathbf{c}\|^2}{2\sigma^2}} \tag{4}$$

The non-focused pixels are blended with a Gaussianblurred version of the original image.

$$Gaussian(x,y) = \frac{1}{2\pi\sigma^2} e^{-\frac{x^2+y^2}{2\sigma^2}}$$
 (5)

Table 4 provides the statistics of the proposed Action-Genome dataset.

Statistic	Value
Images	615,805
Action classes	740
Object classes	4812
Relation classes	225,609

Table 4. Details of the Action-Genome Dataset.

7.1. Data Curation

We arrive at a condensed list of object, action, and relation classes. For datasets like Kinetics-400, MMT etc., the

dataset provides us with action classes, which we directly use. For the other datasets, we curate the action classes manually into groups. For instance the actions "taking a photo", "taking a photograph", "taking a selfie" and "taking photos" are all combined into a single action of "taking a photograph" (Figure 7).

In the generated list of objects, for which we have bounding boxes, we observed that several related objects were present as distinct items. Another problem is the collection of multiple different objects together in the same bounding box, leading to that label having multiple unrelated nouns in the same string, just because they are in the same bounding box. To combat this, we first run a pass on the generated bounding box labels, and the labels that generated the focused regions according to the ground truth relations, and come to a reduced list of objects by taking an intersection of the objects on each sample identified by VLMs from all stages, and the union of all of these intersections.

Even after this reduction (Figure 6), we can see a list of various objects, where certain related items are identified as distinct. Further, some objects appeared in both *singular* and *plural* forms, while others included *adjectives* or *color descriptors* in their names. To tackle these problems, we implemented a three-step filtering process.

First, we removed the adjectives and color descriptors to standardize the object names. We use a predefined list of common color terms to remove the color descriptors. Additionally, we use the NLTK library [3] to identify and remove tokens tagged as adjectives by the NLTK part-of-speech (POS) classifier. Next, we remove the plural forms of objects that appeared in both singular and plural forms.

To group related objects together, we first use the BERT [8] model to get semantically meaningful embeddings for the objects. On these embeddings, we use HDBSCAN (Hierarchical Density-Based Spatial Clustering of Applications with Noise) [4] for clustering. HDBSCAN assigns clusters based on density of the data points. A *mutual reachability distance*, defined as:

$$d_{\text{mreach-}k}(a, b) = \max\{\text{core}_k(a), \text{core}_k(b), d(a, b)\}$$

is calculated to incorporate density into the distance calculation. We have used the *cosine* metric for distance calculation.

Finally, we manually label grouped objects to give them semantically meaningful labels. For example, the group containing "garbage truck", "trash can", "waste bin", "trash bag", "trash bin", and "garbage bags" is labeled "waste

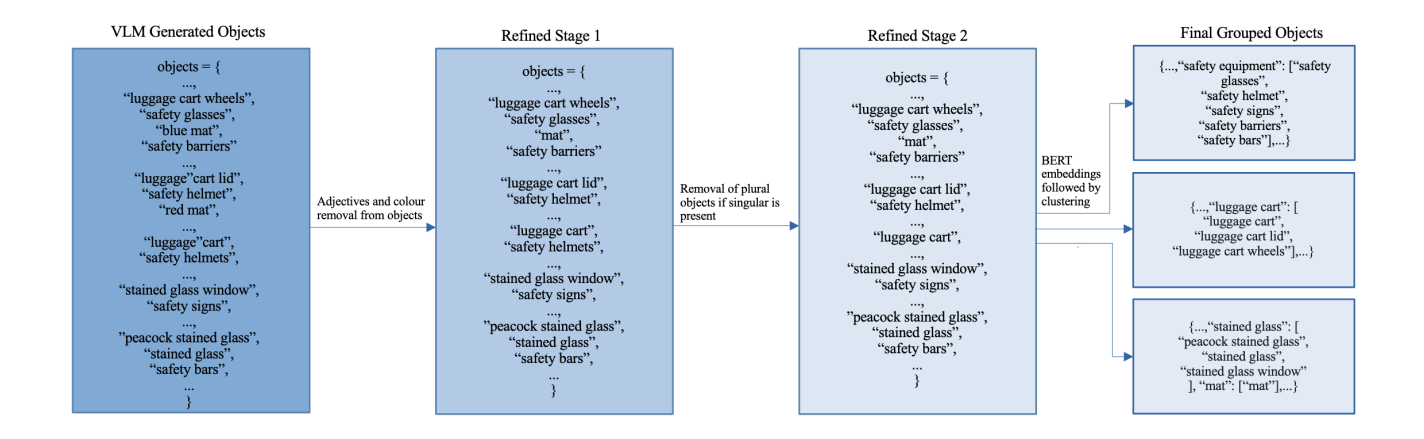


Figure 6. Object processing pipeline, illustrating the refinement from raw VLM-generated object strings to final grouped object classes by removing adjectives and color descriptors, eliminating redundant plural forms, and clustering semantically similar objects using BERT embeddings and HDBSCAN.

	Predica	ate Class	ification	Scene Graph Classification			
Model	R@1	R@5	R@10	R@1	R@5	R@10	
PyramidCLIP [14]	30.33	63.94	78.37	25.64	56.52	71.38	
ScenarioCLIP w/o KD	32.60	64.48	77.47	29.56	59.87	73.17	
ScenarioCLIP	34.84	67.53	80.14	31.34	62.58	<i>75.57</i>	

Table 5. Results for predicate classification and scene graph classification.

management".

In the generated relations, we observed that several semantically equivalent relations are generated, differing only by a stopword. For instance, "air conditioner mounted wall" and "air conditioner mounted on wall" have the same semantic meaning, but differ only by a stopword. To refine the relations, we first extract the $(object_1, relation, object_2)$ from all relations. Next, we replace $object_1$ and $object_2$ with their corresponding group label, if they were clustered into a group during object clustering. We further remove the stopword from the relation part of the triplet to handle the issue of semantically equivalent relations differing only by a stopword. Using this processed triplet, we check if another relation that has the same triplet exists. If it does, we keep one of the relations and discard the other (Figure 8). We further curate the classes manually.

8. Experiments

8.1. Implementation Details

8.1.1. Pre-training Stage

All ScenarioCLIP variants are pretrained on the Action-Genome dataset for 12 epochs using the AdamW optimizer [38]. We use a base learning rate of 2×10^{-5} ,

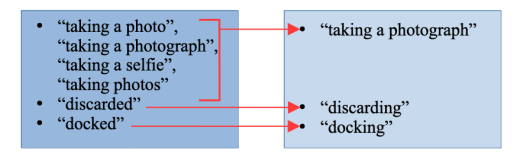


Figure 7. Action processing and consolidation, where diverse raw action phrases are normalized and merged into a smaller set of canonical action labels.

 $\beta=(0.9,0.999),\ \varepsilon=10^{-8}$ and a weight decay of 0.2 for all trainable parameters in the vision-language backbone and contrastive loss modules. We employ a learning-rate schedule with a linear warm-up over the first 10% of the total optimization steps, where the learning rate increases from 10^{-3} of the base value to the full learning rate, followed by a cosine annealing schedule down to a learning rate floor of 0 for the remaining steps.

For ScenarioCLIP, the learnable distillation temperature parameter in the student-teacher loss is optimized as a separate parameter group with the same AdamW [38] optimizer, using a learning rate of $0.1\times$ the base learning rate and no weight decay, which we found to stabilize training. During

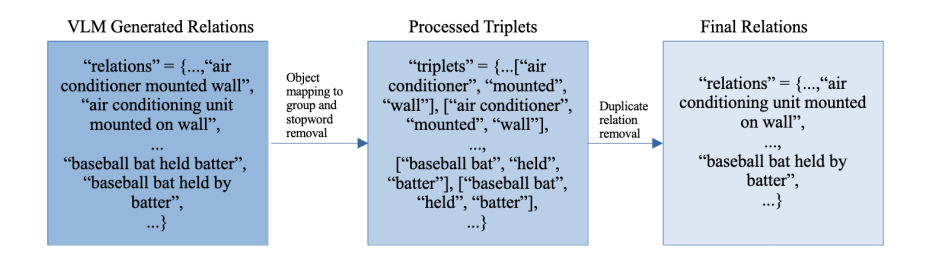


Figure 8. Relation processing pipeline. Raw VLM-generated relation strings are converted into relation triplets by mapping objects to groups, removing stopwords, and collapsing duplicate triplets into a final relation set.

	Frozen	Encoder		Trainable Encoder			
Model	Dice Coefficient (†)	IoU (†)	$MAE(\downarrow)$	Dice Coefficient (†)	IoU (↑)	MAE (↓)	
PyramidCLIP [14]	0.6378	0.5269	0.1535	0.5971	0.4858	0.1625	
ScenarioCLIP w/o KD	0.6340	0.5242	0.1512	0.6085	0.4962	0.1643	
ScenarioCLIP	0.6230	0.5145	0.1509	0.6010	0.4892	0.1636	

Table 6. Relation localization performance for frozen vs. trainable visual encoders.

	Actions				Objects			Relations		
λ_{KD} schedule	Top-1	Top-5	Top-10	Top-1	Top-5	Top-10	Top-1	Top-5	Top-10	
Fixed-1	57.63	75.02	79.99	51.86	64.43	68.30	19.56	37.03	45.86	
Fixed-10	57.26	75.11	80.21	48.97	64.31	68.21	19.49	36.87	45.71	
Anneal $1 \to 0$	57.15	75.23	80.39	52.28	64.52	68.40	19.47	37.03	45.95	
Anneal $10 \rightarrow 0$	57.23	75.24	80.44	51.74	64.44	68.36	19.52	36.90	45.81	

Table 7. Zero-shot image \rightarrow text retrieval on the Action-Genome dataset under different choices of the distillation weight λ_{KD} .

pretraining, we also maintain an exponential moving average (EMA) teacher of the student parameters with a decay of 0.9995 and a warm-up of 2000 optimization steps before EMA updates are applied.

8.1.2. Linear-Probe

For linear probing, we freeze all parameters of the pretrained backbone and train only a lightweight classification head attached to the frozen visual encoder. Depending on the evaluation task (action, object, or relation classification), we add a single linear layer of size $512 \rightarrow C$, where C is the number of classes for that task.

The linear head is trained using a cross-entropy loss over the Action-Genome labels. We train the models for 6 epochs with the AdamW [38] optimizer and a learning rate of 2×10^{-5} .

8.1.3. Object Detection

For object detection, we use Faster R-CNN [49] with our pretrained encoders serving as backbones. As described in the main paper, PyramidCLIP [14] uses a single unified visual encoder for both the RPN and RoI heads, whereas Sce-

narioCLIP employs separate encoders: the global visual encoder provides RPN features for proposal generation, and the object visual encoder supplies the RoI features for classification and regression. In all cases, backbone features are converted into multi-scale inputs via a lightweight convolutional pyramid followed by an FPN.

The detector is trained for 10 epochs on the Action-Genome dataset using AdamW [38] with a backbone learning rate of 1×10^{-5} , and larger learning rates for the FPN and detection heads. We apply a 5% warm-up followed by cosine decay. The dataset's pronounced long-tailed distribution (with 4812 object classes) necessitates careful sampling. We therefore adopt an Instance-Aware Sampler [67]: for each image, we compute a rarity score based on both the number of images containing a class and the total instance count of that class. Sampling weights are assigned inversely to this joint frequency (with clipping), increasing exposure to tail-class images while preserving training stability. In addition, for categories with fewer than 50 training instances, we apply class-targeted Copy-Paste augmentation to further increase their occurrence during training.

As is common for long-tailed object detection tasks, dur-

ing inference we set the box score threshold to 10^{-4} , apply NMS at 0.5, and allow up to 300 detections per image.

8.1.4. Predicate Classification & Scene-Graph Classification

For predicate classification (PredCls), we use the groundtruth bounding boxes and categories of the two objects involved in each annotated relation, denoted $object_1$ and $object_2$. We first build a predicate vocabulary \mathcal{P} from a subset of approximately 700 predicates in the training set, and restrict evaluation to test relations whose predicate lies in this subset. At test time, for every relation we extract a relation feature from the union of the object1 and object2 regions using the relation visual encoder, and construct text features for all candidate triplets $(object_1, predicate, object_2)$ with $predicate \in \mathcal{P}$ using the relation text encoder. Predicate scores are obtained as cosine similarities between the visual relation feature and each text feature, and predicates are ranked accordingly. We report Recall@K for $K \in \{1, 5, 10\}$ over the selected test relations.

For scene graph classification (SGCls), the setup is similar to predicate classification, except that the object categories are also predicted. We build an object vocabulary $\mathcal C$ from the training split and, for each object crop, obtain a visual embedding using the object encoder. Each object is classified by comparing its embedding against text embeddings for all $c \in \mathcal C$, yielding predicted labels for $object_1$ and $object_2$. These predicted labels replace the ground-truth categories when forming relation prompts $(object_1, predicate, object_2)$. Predicates are then scored and ranked as above, and we again evaluate using Recall@K for $K \in \{1, 5, 10\}$.

As shown in Table 5, ScenarioCLIP clearly improves predicate classification over PyramidCLIP [14], with gains of +4.51/+3.59/+1.77 points in R@1/5/10, respectively. This demonstrates that, even when the object categories are given, our relation encoder produces more discriminative visual-text alignment than PyramidCLIP [14].

In the SGCls setting, where both object categories and predicates are predicted, ScenarioCLIP also consistently outperforms PyramidCLIP [14], with gains of +5.70/+6.06/+4.19 points in R@1/5/10, respectively. These improvements indicate that ScenarioCLIP not only enhances predicate recognition, but also learns a stronger object classifier than PyramidCLIP.

8.1.5. Relation Localization

To evaluate how well the relation encoder captures the spatial extent of an interaction, we train a lightweight decoder to predict a dense *relation mask*. For each annotated $(object_1, relation, object_2)$ triple in Action-Genome, we construct a focused input image by zeroing out all pixels outside the union of the $object_1$ and $object_2$ bounding

boxes, and use the corresponding relation mask provided in the dataset as the supervision signal.

The visual backbone is the pretrained relation visual encoder. Given the focused image, we run the encoder, discard the class token, and reshape the remaining patch tokens into a $h \times w$ feature map. This map is passed through a small convolutional decoder (Conv3 \times 3-256-ReLU-Conv3 \times 3-64-ReLU-Conv1 \times 1-1) to produce patch-level logits, which are bilinearly upsampled back to the image resolution and squashed with a sigmoid to obtain a probability mask.

We optimize the decoder using an ℓ_2 loss between the predicted and ground-truth masks with Adam (learning rate 10^{-4}). We consider two variants: (i) *Frozen*, where the relation encoder is kept fixed and only the decoder is trained, and (ii) *Trainable*, where both encoder and decoder are updated.

Table 6 summarizes relation localization performance. With frozen encoders, PyramidCLIP [14] attains slightly higher Dice and IoU than ScenarioCLIP, which is consistent with the fact that its entangled backbone is trained jointly on global images, object crops, and relation masks. Scenario-CLIP achieves the lowest MAE, indicating that its dedicated relation encoder recovers relation regions with very similar pixelwise accuracy.

When we allow the visual encoders to be updated for this task, ScenarioCLIP becomes competitive or better than PyramidCLIP [14]. ScenarioCLIP without distillation obtains the best Dice and IoU among all models, while ScenarioCLIP with KD remains close behind. This suggests that, once fine-tuned for relation localization, the disentangled design in ScenarioCLIP can match or surpass the entangled PyramidCLIP [14] backbone, showing that separating relation reasoning does not compromise spatial localization of interactions.

8.1.6. Visualizations

To better understand what the object encoder learns, we visualize where each model attends in the image using a Grad-CAM [53] heatmap. For each test image, we feed the entire image through the object visual encoder and obtain the final ViT token sequence. The first token is the global CLS token, and the remaining tokens correspond to image patches. We interpret the similarity between each patch token and the CLS token as a proxy for how much that patch contributes to the predicted object representation. These similarities are reshaped into an $h \times w$ patch grid, upsampled to the input resolution, and overlaid on the original RGB image using a jet colormap.

Figure 9 compares PyramidCLIP [14], ScenarioCLIP without knowledge distillation, and ScenarioCLIP with knowledge distillation on three images. Since scenes often contain multiple objects, there is no single "correct" attention map. Instead, we qualitatively assess whether the highlighted regions align with the intuitive object of in-

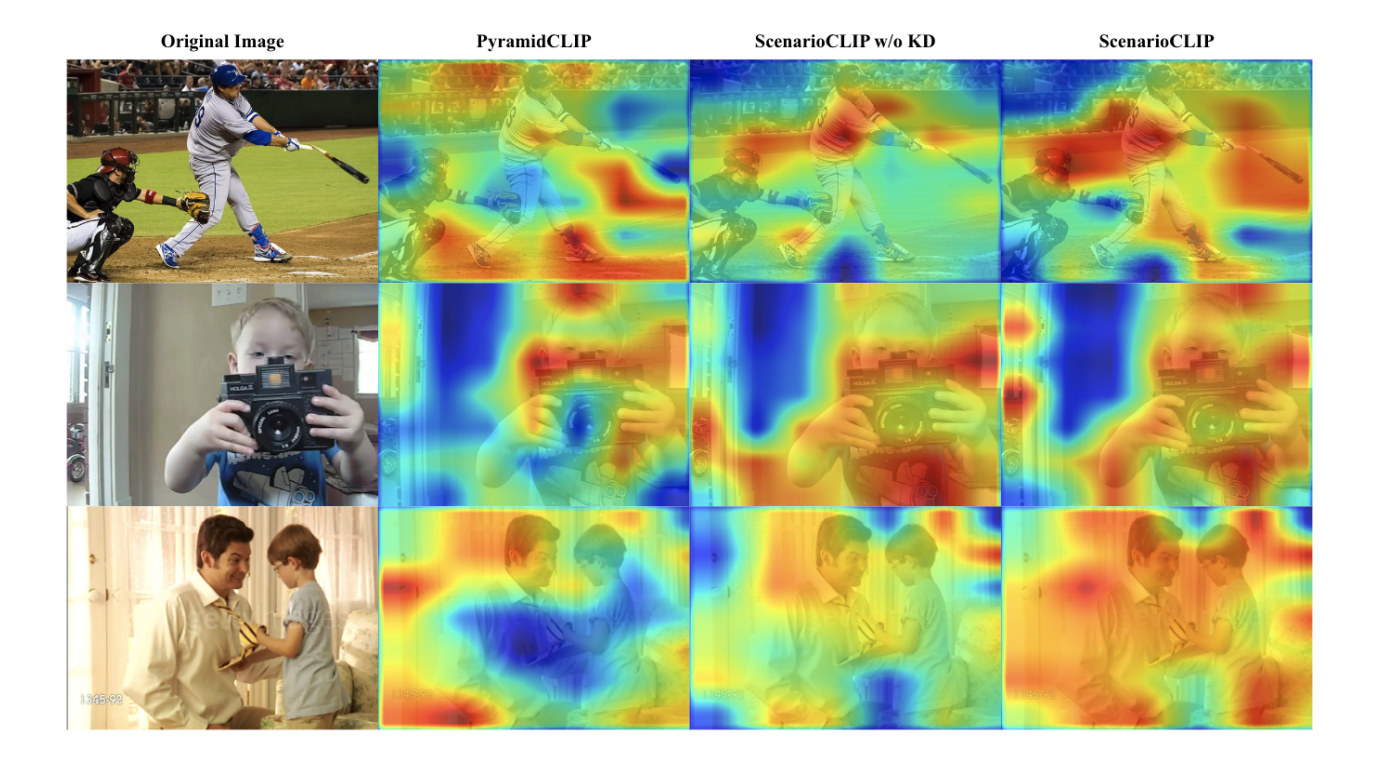


Figure 9. Grad-CAM [53] visualizations of the object encoder for PyramidCLIP [14], ScenarioCLIP w/o KD, and ScenarioCLIP. For each image, we feed the whole frame into the object encoder and compute a patch-level relevance map, which is overlaid on the original image. ScenarioCLIP produces more focused and semantically meaningful activations around the objects and interactions of interest, while PyramidCLIP [14] attends more to background regions.

terest. Across all rows, ScenarioCLIP produces sharper and more localized responses around semantically meaningful regions. In the first image, ScenarioCLIP concentrates on the batter, bat, and catcher rather than diffuse background areas. In the second example, ScenarioCLIP focuses on the camera and the child's hands, while Pyramid-CLIP [14] and ScenarioCLIP w/o KD allocate substantial mass to the background wall. Similarly, in the final image, ScenarioCLIP emphasizes both people and their interaction, whereas the baselines attend more to surrounding clutter (e.g., curtains and background). These visualizations indicate that ScenarioCLIP learns more object-centric, relationaware representations than PyramidCLIP [14].

8.2. More Ablations

As mentioned in the main paper, the objective function combines the knowledge distillation loss \mathcal{L}_{KD} and the contrastive alignment loss \mathcal{L}_{CA} :

$$\mathcal{L}_{\text{total}} = \lambda_{KD} \cdot \mathcal{L}_{KD} + \lambda_{CA} \cdot \mathcal{L}_{CA}, \tag{6}$$

where λ_{KD} and λ_{CA} are weighting coefficients that balance the contributions of the two terms.

We study the effect of the distillation weight λ_{KD} using four settings:

- 1. **Fixed-1:** $\lambda_{KD} = 1$ for all epochs.
- 2. **Fixed-10:** $\lambda_{KD} = 10$ for all epochs.
- 3. Anneal $1 \to 0$: λ_{KD} is initialized to 1 and annealed to 0 over training.
- 4. **Anneal** $10 \rightarrow 0$: λ_{KD} is initialized to 10 and annealed to 0 over training.

All experiments reported in the main paper use the Fixed-1 setting, i.e., $\lambda_{KD}=1$ throughout training. For the annealed variants we parameterize training progress as $p=(e+1)/E\in[0,1]$, where e is the current epoch and E is the total number of epochs, and partition training into three phases with breakpoints $p_1=0.4$ and $p_2=0.7$. The weight λ_{KD} is then defined as

$$\lambda_{KD}(p) = \begin{cases} \lambda_{\text{start}}, & p \leq p_1, \\ \lambda_{\text{mid}} + \frac{\lambda_{\text{start}} - \lambda_{\text{mid}}}{2} \left(1 + \cos(\pi t_1) \right), & p_1 p_2. \end{cases}$$
(7)

where $t_1=\frac{p-p_1}{p_2-p_1}$ and $t_2=\frac{p-p_2}{1-p_2}$. We set $\lambda_{\rm end}=0$ and use $(\lambda_{\rm start},\lambda_{\rm mid})=(1,0.5)$ for the "Anneal $1\to 0$ " configuration and $(\lambda_{\rm start},\lambda_{\rm mid})=(10,1)$ for "Anneal $10\to 0$ ". Thus, λ_{KD} is held constant for the first 40% of training and then smoothly decayed to 0 by the end. Zero-shot

image \rightarrow text retrieval accuracy for these four settings are shown in Table 7.